

Relationship between central autonomic effective connectivity and heart rate variability: A Resting-state fMRI dynamic causal modeling study

Liangsuo Ma ^{a,b,*}, Larry D. Keen II ^c, Joel L. Steinberg ^{a,b,i}, David Eddie ^{d,e}, Alex Tan ^f, Lori Keyser-Marcus ^b, Antonio Abbate ^e, F. Gerard Moeller ^{a,b,g,h,i}

^a Institute for Drug and Alcohol Studies, Department of Psychiatry, Virginia Commonwealth University, 203 East Cary Street, Suite 202, Richmond 23219, VA, United States

^b Department of Psychiatry, Virginia Commonwealth University, VA, United States

^c Department of Psychology, Virginia State University, VA, United States

^d Recovery Research Institute, Center for Addiction Medicine, Massachusetts General Hospital, MA, United States

^e Department of Psychiatry, Harvard Medical School, MA, United States

^f Berne Cardiovascular Research Center, University of Virginia, Charlottesville, VA, United States

^g Department of Pharmacology and Toxicology, Virginia Commonwealth University, VA, United States

^h Department of Neurology, Virginia Commonwealth University, VA, United States

ⁱ C. Kenneth and Dianne Wright Center for Clinical and Translational Research, Virginia Commonwealth University, VA, United States

ARTICLE INFO

Keywords:

Heart rate variability
Heart rate, autonomic
Resting state
Dynamic causal modeling
Effective connectivity

ABSTRACT

The central autonomic network (CAN) serves as a regulatory hub with top-down regulatory control and integration of bottom-up physiological feedback via the autonomic nervous system. Heart rate variability (HRV)—the time variance of the heart's beat-to-beat intervals—is an index of the CAN's affective and behavioral regulatory capacity. Although neural functional connectivities that are associated with HRV and CAN have been well studied, no published report to date has studied effective (directional) connectivities (EC) that are associated with HRV and CAN. Better understanding of neural EC in the brain has the potential to improve our understanding of how the CAN sub-regions regulate HRV. To begin to address this knowledge gap, we employed resting-state functional magnetic resonance imaging and dynamic causal modeling (DCM) with parametric empirical Bayes analyses in 34 healthy adults (19 females; mean age = 32.68 years [$SD = 14.09$], age range 18–68 years) to examine the bottom-up and top-down neural circuits associated with HRV. Throughout the whole brain, we identified 12 regions associated with HRV. DCM analyses revealed that the ECs from the right amygdala to the anterior cingulate cortex and to the ventrolateral prefrontal cortex had a negative linear relationship with HRV and a positive linear relationship with heart rate. These findings suggest that ECs from the amygdala to the prefrontal cortex may represent a neural circuit associated with regulation of cardiodynamics.

1. Introduction

Affective and behavioral regulation rely heavily on bidirectional brain-body communication, which influences moment-to-moment neurological and physiological changes that support responses to situational demands (Beissner et al., 2013; Benarroch, 1997). Although several brain networks support affective and behavioral regulation, the central autonomic network (CAN) regulates dynamic physiological control via the autonomic nervous system (Sklerov et al., 2019). In turn, the body constantly feeds information about physiological states back to the CAN via diverse sensory afferents (Critchley, 2005). In a continuous

loop, this information then influences subsequent CAN output (Goldstein, 2001).

Key components of the CAN include cortical structures such as the anterior cingulate cortex, insula, and prefrontal cortices, and subcortical structures such as the amygdala, hippocampus, and hypothalamus (Arnsten, 2009; Beissner et al., 2013). In the presence of threat or other salient information, subcortical structures such as the amygdala exert excitatory influence on CAN cortical areas through the ascending pathways (Barbas and Zikopoulos, 2007; Chen et al., 2008; Everitt et al., 2000; Gabbott et al., 2006; Nikolin et al., 2017; Smith and Torregrossa, 2021). Conversely, cortical structures such as the anterior cingulate

* Corresponding author.

E-mail address: Liangsuo.ma@vcuhealth.org (L. Ma).

cortex have been reported to exert top-down inhibitory control over subcortical regions (including the amygdala) through descending pathways, supporting regulation of emotional states and behavior (Kujawa et al., 2016; Lane et al., 2009; Thayer and Lane, 2009; Wager et al., 2009).

Although the CAN controls an array of important psychophysiological functions (Benarroch, 1993; Critchley, 2009), its control of the cardiovascular system via autonomic nervous system pathways is perhaps the most important. Through sympathetic and parasympathetic innervation of the heart, the CAN affects fine-grained changes in heart rate in response to situational demands (Appelhans and Luecken, 2006; Benarroch, 1993). This neurocardiac modulation is reflected by dynamic changes in the heart rate and by the time-variance of the heart's beat-to-beat intervals known as heart rate variability (HRV) (Shaffer and Ginsberg, 2017; Shaffer et al., 2014). Higher HRV, reflecting greater physiological and psychophysiological flexibility, is typically associated with health, while lower HRV is commonly observed in individuals experiencing psychological and physiological disease states (Pham et al., 2021; Young and Benton, 2018).

HRV is primarily driven by vagally mediated parasympathetic innervation of the heart, which serves as a brake that counters tonic cardiac sympathetic innervation (Laborde et al., 2017; Mayhugh et al., 2018). There are numerous indices of HRV which are thought to reflect varying degrees of parasympathetic and sympathetic influences on cardiodynamics, but most measures of HRV primarily reflect parasympathetic control (Kim et al., 2018). Heart rate, on the other hand, is thought to reflect both parasympathetic and sympathetic influences on the heart (Wehrwein et al., 2016).

Numerous resting-state fMRI investigations have explored the relationship between brain functional connectivity and HRV. For instance, Sakaki et al. (2016) identified a positive correlation between HRV and the strength of functional connectivity between the amygdala and the medial prefrontal cortex. Further, Chand et al. (2020) showed a dynamic temporal interplay between HRV and the strength of functional connectivity within the CAN, salience network, and default mode network, with fluctuations related to varying conditions like stress. Lee et al. (2021) reported a decrease in high-frequency HRV in individuals with internet gaming disorder during real-time gaming, linked to functional connectivity between the dorsolateral prefrontal cortex and ventrolateral prefrontal cortex (inferior frontal gyrus). Additionally, Schumann et al. (2021) observed temporal covariation between HRV changes and dynamic shifts in prefrontal functional connectivity, particularly involving the middle cingulate cortex, left anterior insula, right amygdala, supplementary motor area, and dorsal and ventral lateral prefrontal regions. Collectively, these studies reinforce early work suggesting that HRV is influenced by the morphology, activity, and functional connectivity of brain structures in the CAN (Matusik et al., 2023).

However, no prior published research has utilized newer effective-connectivity-based methodologies to study the nuances of how the CAN regulates HRV. Investigating the effective (directional) connectivity of the CAN could lead to the identification of neural targets for biobehavioral interventions that help individuals to regulate emotions and behaviors more effectively. In this study, we conducted an effective connectivity (EC) analysis of resting-state fMRI data from 34 healthy adults. In contrast to functional connectivity, which captures the temporal correlations among spatially separated brain regions, EC assesses the causal, directional influence of one brain region's activity on another (Friston, 2011). We posited that the EC approach would be particularly useful for identifying top-down and bottom-up CAN brain neural pathways which influence cardiodynamics.

Dynamic causal modeling (DCM) (Friston et al., 2003, 2019) has been used to estimate EC within hypothesized networks modeled at the neuronal level (Friston et al., 2003). DCM was originally developed for task fMRI (Friston et al., 2003). Task-fMRI-based DCM is a model for assessing how neuronal ECs change under experimental conditions (or

in response to stimuli) by generating a hemodynamic time series within each node (i.e., brain region). In this study, we used spectral-DCM (Friston et al., 2014), which was developed for inferring ECs within resting-state fMRI data. Unlike task-fMRI-based DCM, spectral-DCM is a model of neuronal (directional) ECs that predict the observed statistical dependencies between nodes (Friston et al., 2014).

In order to determine which brain regions should be included in our spectral-DCM analysis, we used regression-DCM (Frassle et al., 2020, 2017) throughout the whole brain to find the brain regions most likely related to HRV. Due to several key modifications and simplifications (Frassle et al., 2018, 2017), regression-DCM has exceptional computational speed relative to standard DCM (Frassle et al., 2018, 2017), making regression-DCM a feasible approach for the analysis of ECs within large-scale networks (Frassle et al., 2020, 2018, 2021b).

In this study, we tested the following hypotheses. First, given the established roles of the amygdala and prefrontal regions in CAN and cardiac functions, we predicted that the amygdala and prefrontal regions would be identified as relevant nodes by our regression-DCM analysis (Hypothesis 1). Next, based on existing understanding of how the CAN regulates HRV, we predicted that greater HRV would be associated with greater strength of ECs from the prefrontal regions to the amygdala (i.e., greater top-down control; Hypothesis 2A). Previous work has also shown that in the presence of threat or other salient information, the amygdala exerts excitatory influence on prefrontal regions to promote conscious awareness and attention (Barbas and Zikopoulos, 2007; Chen et al., 2008; Everitt et al., 2000; Gabbott et al., 2006; Nikolin et al., 2017; Smith and Torregrossa, 2021). The amygdala is typically regarded as part of the salience network (Menon and Uddin, 2010; Seeley, 2019) and processes changes in the body's internal state and thus serves as an important center for interoception (Gothard and Fuglevand, 2022; Grundemann et al., 2019). In this context, the amygdala and prefrontal regions process background information in a bottom-up manner (LeDuke et al., 2023). Background information from the brain's resting-state default mode network may concurrently be sent from the amygdala to prefrontal regions (bottom-up delivery of information) without triggering activation of prefrontal regions for attention or conscious awareness. Based on this reasoning, we hypothesized that greater HRV would be associated with lower ECs from the amygdala to the prefrontal regions (i.e., less consolidation of fear memory) (Hypothesis 2B). Finally, because heart rate is under both parasympathetic inhibitory and sympathetic excitatory control (He, 2020; White and Raven, 2014), and is typically inversely associated with HRV (Kazmi et al., 2016; Monfredi et al., 2014), we hypothesized that ECs displaying a positive linear relationship with HRV would exhibit an inverse linear relationship with heart rate (Hypothesis 3).

2. Methods and materials

2.1. Participants

Data for this study were sourced from the Phenotyping Assessments Battery (PhAB) Feasibility and Validation Study in Non-Intoxicated Drug Users (Keyser-Marcus et al., 2021), a project funded by the National Institute on Drug Abuse (NIDA; U54DA038999). Ethical approval was obtained from the Virginia Commonwealth University local committee for the protection of human subjects, and all procedures adhered to the ethical guidelines outlined in the Declaration of Helsinki (Rickham, 1964). Written informed consent was obtained from all participants. The present investigation utilized data exclusively from the PhAB study's healthy control participants.

Inclusion criteria for control participants in the PhAB study included being age 18 to 70 years and proficient in English. Exclusion criteria included current mental health problems (e.g., psychosis, mania, suicidal/homicidal ideation), substance use disorder, positive results on substance use screenings prior to fMRI scans, left-handedness, history of seizures (except for febrile seizures during childhood without sequelae),

prolonged loss of consciousness due to traumatic injury, any condition that could compromise the safety or success of the study, the presence of metal fragments in the body, fear of confined spaces, current pregnancy or nursing, and definite or suspected clinically significant brain abnormalities observed on MRI scans.

2.2. Heart rate variability assessment

Pulse photoplethysmograph recordings were obtained during the resting-state fMRI scan using the Philips Invivo pulse-oximeter, with a sampling rate of 496 hertz. Pulse photoplethysmograph recordings were post-processed offline (removing noise and artifact) using the PhysIO Toolbox for automatic cardiac cycle peak detection and determination of heart rate (Kasper et al., 2017). The output from the PhysIO toolbox, consisting of the timing of each cardiac cycle peak, was then entered into Kubios HRV software (Tarvainen et al., 2014). Beats were corrected for artifact and ectopic beats via automatic correction algorithms. HRV metrics were selected in accordance with international recommendations for short-term HRV (Laborde et al., 2017; Malik et al., 1996). All participants were engaged in spontaneous breathing; rate of respiration was not measured.

We included two distinct, parasympathetically-driven HRV metrics: the root mean square of successive differences (RMSSD), and high-frequency HRV (HF HRV). RMSSD is a widely employed measure in fMRI research (Chand et al., 2020; Chang et al., 2013; Lee et al., 2021; Sakaki et al., 2016; Schumann et al., 2021; Young et al., 2019). HF HRV, reflecting the relative power within the high-frequency band (0.15–0.4 hertz), was chosen for its closer association with respiration (Stein et al., 1994), offering potential distinction from RMSSD. As the two types of HRV scores were derived from different normal distributions (i.e., the two HRV scores had different means and different scales of standard deviation), the scores were converted into standard z-scores for subsequent analyses examining the relationship between ECs and HRV. Standard z-scores can improve the interpretability of regression coefficients (Schielzeth, 2010) by allowing the estimation of standardized slopes, which are comparable in magnitude between different linear regression analyses (Schielzeth, 2010).

2.3. fMRI data acquisition

T1-weighted MPRAGE and resting-state fMRI data were acquired using a 3 T MRI scanner (Philips Ingenia, Best, the Netherlands) equipped with a phase-array SENSE 32-channel receiver head coil. During the resting-state fMRI scan, participants were instructed to relax, maintain their focus on a plus sign (+) displayed on a screen, and stay awake. Blood oxygen level dependent (BOLD) signal was measured using a T2* gradient-echo echoplanar-imaging sequence with the following parameters: repetition-time=1.625 s, echo-time=30 milliseconds, multiband factor = 3, in-plane SENSE factor = 1.5, 45 slices, slice-thickness=2.5 mm, 0.3 mm gap, field-of-view=[240 × 240] mm, in-plane resolution=[2.5 × 2.5] mm, flip-angle=52 deg, 384 vol, with a total duration of 10 min and 24 s.

2.4. Resting-state fMRI data preprocessing

We followed a preprocessing procedure similar to Ma et al. (2021) and Woisard et al. (2021). This included initial removal of BOLD signal outliers for each voxel, defined as fMRI signals that were 6 standard deviations greater than the mean signal in the run for that voxel. Each signal outlier was replaced with the average of the two nearest non-outlier values for that voxel (the first one previous and the first one after), using the Analysis of Functional NeuroImages (AFNI) (Cox, 1996) “3dDespike” command with the “localedit” option. After removal of signal outliers, other preprocessing procedures included correction for slice timing, motion correction, registration to the T1-weighted anatomical scan, and spatial smoothing. The steps for quality control

for spatial displacement and BOLD signal artifacts due to head motion were conducted in the following order. 1) Following Pruij et al. (2015a), anatomical (spatial) displacement due to head motion of each volume in the run was corrected using FSL MCFLIRT (Jenkinson et al., 2002; Woolrich et al., 2004), which spatially realigned each volume to the middle volume in the run. The amount of spatial displacement in the run was reported by this software in terms of mean framewise displacement (mean FD), defined in Jenkinson et al. (2002). 2) Quality control for excessive amounts of spatial displacement due to head motion was conducted by excluding subjects based on the following stringent criteria proposed by Parkes et al. (2018), which excluded subjects who had either (a) a mean FD greater than 0.20 mm, or (b) a frequency of occurrence of large FDs (i.e., FDs greater than 0.25 mm) >20 percent of the total number of FDs in the run, or (c) any FD greater than 5 mm, or (d) >4 min of FDs greater than 0.25 mm. After exclusion of subjects who had excessive levels of spatial displacement due to head motion based on these criteria, the resulting FD values were small (0.09 ± 0.03 mm, ranging from 0.05 to 0.19 mm). 3) Correction of artifacts in the BOLD signal due to head motion was conducted using ICA-AROMA (Pruij et al., 2015b). These steps essentially followed the steps in Pruij et al. (2015a) for the ICA-AROMA technique, with the exception that the criteria that we used in Step 2 above were somewhat more stringent for excluding subjects with excessive spatial displacement than similar criteria in Pruij et al. (2015a). Pruij et al. (2015a) compared a variety of different methodologies to control for head motion and found that the combination of the following steps (spatial realignment, exclusion of subjects who had excessive levels of spatial displacement due to head motion, and ICA AROMA correction of motion-related artifacts in the BOLD signal), led to improved reproducibility of resting-state networks, preservation of the signal of interest, and decreased loss of total degrees of freedom compared to other methodologies (Pruij et al., 2015a). Signal denoising from cerebrospinal fluid and white matter components was performed with the aCompCor procedure (Behzadi et al., 2007) implemented in CONN software (Whitfield-Gabrieli and Nieto-Castanon, 2012). A high pass filter with a cutoff period of 125 s was applied as a final denoising step. Finally, the T1-weighted anatomical scan and denoised fMRI timeseries were transformed into MNI space using the FSL FNIRT non-linear transformation.

2.5. Dynamic causal modeling (DCM)

The parameters within DCM serve to quantify the directed influences, or ECs, among various neuronal populations. These ECs are estimated from fMRI data employing Bayesian statistical methods (Friston et al., 2003, 2019). To facilitate group-level analyses, advanced DCM analytical techniques have been developed and are implemented in the SPM12 software (<http://www.fil.ion.ucl.ac.uk/spm/>). These techniques encompass Bayesian model selection (Stephan et al., 2009), Bayesian model averaging, comparison of DCM families (Penny et al., 2010), DCM network discovery (Friston et al., 2011; Friston and Penny, 2011), and parametric empirical Bayes analysis (Friston et al., 2016). Traditional fMRI-based DCM is typically employed for the analysis of small networks, often consisting of fewer than 10 nodes, primarily due to computational constraints associated with the intricate modeling processes (Seghier and Friston, 2013).

The advantage of DCM was underscored by a recent study, which employed a substantial dataset of resting-state fMRI data and detected diurnal variations in the hemodynamic response (Vaisvilaite et al., 2022). Notably, this time-dependent variability had no discernible effect on the results of the DCM EC analysis (Vaisvilaite et al., 2022). In addition, DCM employs Bayesian posterior inference, which mitigates statistical Type I errors associated with multiple comparisons in ECs (Friston et al., 2003; Friston and Penny, 2003; Van Overwalle et al., 2019). Furthermore, the reliability of EC measured through DCM analysis outperformed that of functional connectivity for strong connectivities in both task-based and resting-state fMRI (Frassle and Stephan,

2022).

2.5.1. Regression-DCM

Regression-DCM has exceptional computational speed (Frassle et al., 2018, 2017), rendering it highly suitable for the analysis of ECs within large-scale networks exceeding 100 nodes (Frassle et al., 2020, 2018, 2021b). The speed of regression-DCM is achieved through several key modifications and simplifications (Frassle et al., 2018, 2017) when compared to standard DCM: 1) Conversion of hidden neuronal dynamics from the time domain to the frequency domain using Fourier transformation, 2) replacement of the nonlinear hemodynamic response model with a linear counterpart, 3) consideration of independent connectivity parameters targeting different brain regions, and 4) utilization of Bayesian conjugate priors, ensuring that the posterior and prior distributions belong to the same probability distribution family. In this study, we employed regression-DCM for the exploratory identification of key nodes, which served as a precursor to our main analysis using spectral-DCM. We opted for regression-DCM because of its simplicity, established face validation (Frassle et al., 2017), and prior successful application in resting-state fMRI (Frassle et al., 2020).

2.5.2. Spectral-DCM

Spectral-DCM was purposefully developed by the authors of DCM for inferring ECs within resting-state fMRI data (Friston et al., 2014). In spectral-DCM, the number of parameters is reduced by applying constraints to the connectivity parameters, grounded in the observed functional connectivity patterns (Razi et al., 2017; Seghier and Friston, 2013). Studies have demonstrated the computational efficiency and suitability of spectral-DCM for analyzing medium-sized networks, both theoretically and practically (Friston et al., 2014; Razi, 2017). For instance, Razi et al. (2017) successfully employed spectral-DCM to analyze a network with 36 nodes. Notably, spectral-DCM is integrated into the SPM12 software, and it can be readily complemented by advanced group-level analytical techniques, such as parametric empirical Bayes (Friston et al., 2016).

The mechanism of spectral-DCM is described in detail in Ma et al. (2024) and Novelli et al. (2024). In brief, the ECs are organized into an $N \times N$ matrix (i.e., the A matrix in the DCM differential state-space equation), where N represents the number of nodes. For off-diagonal elements in the A matrix, the EC unit is hertz, representing the rate of change per second (Zeidman et al., 2019). Given an EC from Region 1 to Region 2, a positive EC indicates excitatory effects, meaning Region 1 enhances the activity in Region 2, while a negative EC indicates inhibitory effects, meaning Region 1 decreases the activity in Region 2 (Zeidman et al., 2019). Diagonal ECs (self-connections) in the A matrix are unitless because they represent the log scaling of parameters controlling self-inhibition within each node, affecting their responsiveness to inputs from other nodes (Zeidman et al., 2019). A higher positive self-connection EC (after log scaling) implies greater inhibition in the node, reducing its responsiveness to inputs from other DCM nodes. Conversely, a more negative self-connection EC (after log scaling) implies lower inhibition in the node, leading to relatively increased responsiveness to inputs from other DCM nodes (Zeidman et al., 2019). Biologically, the parameters of the self-connection ECs regulate the balance between excitatory and inhibitory influences within a region, mediated by interactions between pyramidal cells and inhibitory interneurons (Bastos et al., 2012; Zeidman et al., 2019).

2.6. Dynamic causal modeling analysis procedure

First, we utilized regression-DCM (Frassle et al., 2021a) to explore large-scale network-wide ECs associated with HRV. Subsequently, brain regions identified by regression-DCM were cross-referenced with existing literature (Chand et al., 2020; Lee et al., 2021; Matusik et al., 2023; Sakaki et al., 2016; Schumann et al., 2021) to establish regions of interest (nodes) for the subsequent spectral-DCM analysis (implemented in

SPM12 Revision 7771). A flowchart depicting this procedure is provided in Fig. 1, and detailed steps are outlined below. The selected DCM nodes in this study met the following criteria: 1) selected from an initial comprehensive network consisting of 100 nodes (see Step 1 below for details), 2) highly relevant to HRV measures (see Step 1 below for details), 3) supported by existing literature (see Step 2 below for details), and 4) positioned at locations with the strongest resting-state functional connectivity (see Steps 3 to 5 below for details).

2.6.1. Step 1: exploratory analysis of large network EC using regression-DCM

In this analysis, we conducted the estimation of ECs on a scale of $n = 10,000$ (i.e., a 100×100 matrix) within an initial 100-node DCM network. After the ECs were estimated for all the participants, we examined the correlations between each EC and the measures of HRV across all the participants. As is customary, the nodes for the regression-DCM were derived from an atlas. Specifically, the nodes constituting this 100-node network were defined using the AAL3 atlas (Rolls et al., 2020), as described in more detail in the supplementary information. It is important to note that atlas-based nodes may not perfectly align with the actual functional boundaries (Smith et al., 2011). Therefore, this regression-DCM analysis was regarded as exploratory, and the results obtained were solely used to guide the selection of nodes for the main spectral-DCM analysis.

2.6.2. Step 2: select key brain regions relevant to HRV measures based on the results from step 1 and existing literature

In identifying our brain regions of interest, we first identified the 20 ECs (outputs of the regression DCM) most likely related to the HRV measures. The number of top ECs (i.e., 20), corresponding to a statistical p value of 0.002, was arbitrarily selected. When selecting the number of top ECs, we balanced the tradeoff between including more brain regions likely related to HRV and reducing the number of regions to manage the computational load of spectral-DCM. Within these 20 selected ECs, we identified 12 brain regions that were supported not only by our analysis but also by previous research (Beissner et al., 2013; Chand et al., 2020; Lee et al., 2020; Sakaki et al., 2016; Schumann et al., 2020; Thayer et al., 2012; Valenza et al., 2020; Wadden et al., 2018). See the Supplementary Information for the details. These regions included the left and right ventrolateral prefrontal cortices (VLPFC), right medial prefrontal cortex (mPFC), left and right middle temporal gyri (MTG), supracallosal anterior cingulate cortex (ACC), right insula, right amygdala, right hippocampus, left and right thalamus, and right supramarginal gyrus (SMG). For the mapping of these functional regions to anatomical regions in the AAL3 atlas, please refer to Supplementary Table 4.

2.6.3. Steps 3–5

Steps 3–5 (refer to Fig. 1) were carried out following the procedures outlined in Ma et al. (2021). Specifically, the placement of each DCM node (a sphere with an 8-mm radius) was determined using independent component analysis (ICA), wherein the voxel with the highest functional connectivity within each of the seven resting-state networks was identified: default mode network, salience network, left central executive network, right central executive network, amygdala, hippocampus, and thalamus (step 3; further detailed in the supplementary information). ICA (Hyvärinen, 2013) is a statistical method that extracts independent signals from a set of measurement data. Initially introduced to analyze fMRI data by McKeown et al. (1998) to elucidate the spatial and temporal characteristics of task-induced brain activations, ICA has become an important technique in fMRI data analysis, particularly in resting-state fMRI studies (Smitha et al., 2017). It can be categorized into spatial ICA and temporal ICA (Calhoun et al., 2001), depending on whether extracted signals are spatially or temporally independent, respectively. In this study, spatial ICA was used. Left central executive network and right central executive network were specified separately because previous studies have shown these two networks are often

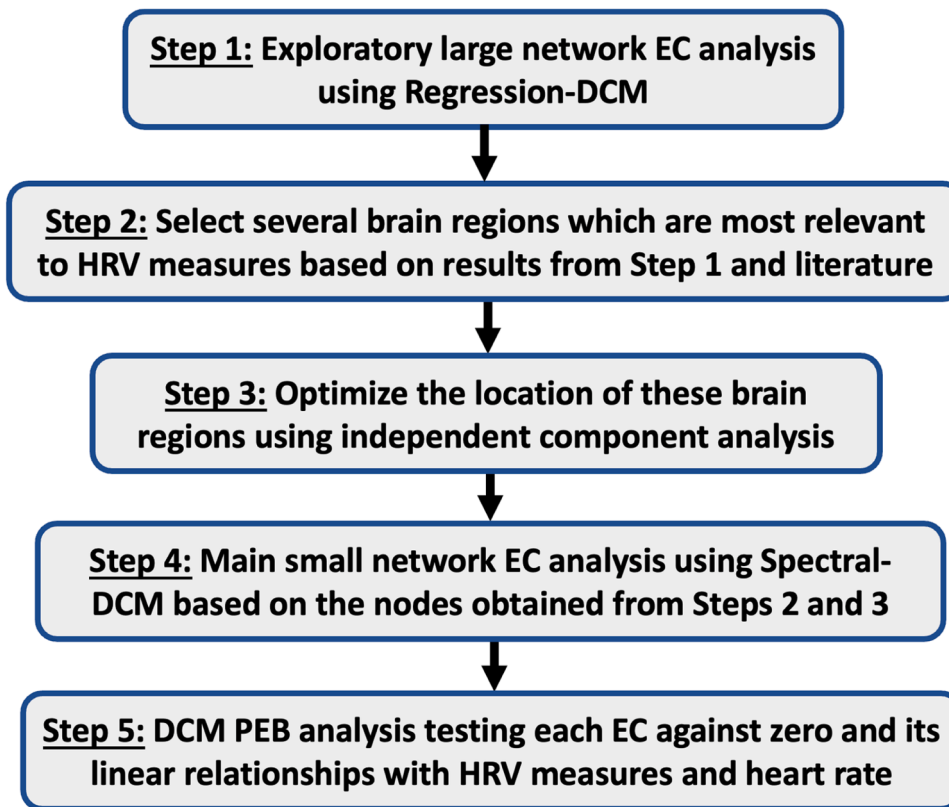


Fig. 1. Flow chart showing the procedure of the DCM analyses used in this study. Note. PEB = parametric empirical Bayes.

found by ICA to be separate (Calhoun and de Lacy, 2017; Smith et al., 2009). After estimating this DCM network using Spectral-DCM (Step 4), group-level DCM analysis was performed using the parametric empirical Bayes approach in Step 5. This included, 1) testing each EC against zero for the entire group and 2) assessing the linear relationship between each EC and each of the non-imaging measures of interest (i.e., RMSSD, HF HRV, and heart rate) using linear regression analysis.

The DCM parametric empirical Bayes group-level analyses were conducted using Bayesian posterior inference (Friston and Penny, 2003) to test whether any of the ECs and any of the linear regression coefficients (*betas*) were different from zero. Unlike frequentist methods, which rely on *p*-values and adjusted thresholds to control for false positives (Type I errors), Bayesian inference estimates the posterior distribution of parameters. By integrating prior knowledge with observed data, Bayesian inference provides a more stable estimation of parameters, thereby mitigating the risk of false positives (Friston and Penny, 2003). In addition, Bayesian inference considers the joint distribution of parameters, rather than treating each comparison in isolation (Friston and Penny, 2003). Thus Bayesian posterior inference in the DCM parametric empirical Bayes group-level analyses is advantageous for avoiding the issue of multiple comparisons (Friston et al., 2003; Friston and Penny, 2003; Van Overwalle et al., 2019). Bayesian posterior probability (Bayesian-PP) was utilized to evaluate the reliability of whether the mean of an EC or the mean of a linear regression coefficient (*beta*) significantly differed from zero at the group level. Bayesian-PP is a conditional probability computed by parametric empirical Bayes using Bayes' rule, integrating available information such as the likelihood function and the prior probability density of the model parameters. Higher Bayesian-PP values indicate greater reliability. In this study, a DCM finding was considered reliable if Bayesian-PP exceeded 0.95, corresponding to a Bayes factor of 3. A Bayes factor of 3 or higher supports accepting a given hypothesis (Baig, 2020).

In our hypothesis testing, we opted to narrow our focus from the entire set of ECs to concentrate on the larger ECs, i.e., the ECs with larger

absolute-value magnitudes. Recent research has provided evidence that resting-state fMRI test-retest reliability is robust for the larger ECs (Frassle and Stephan, 2022). Specifically, from the set of all ECs with Bayesian-PP values above 0.95, we selected those whose absolute value of EC magnitude (measured in hertz, representing the rate of change per second (Zeidman et al., 2019)) ranked in the top half of all absolute values in the set. This selection procedure was based on the approach used in our recent work (Ma et al., 2024) and was intentionally more conservative than the one utilized in Frassle and Stephan (2022) that focused on the top 1000 ECs among 360×360 (129,600) ECs for Glasser parcellation (Glasser et al., 2016) and the top 1000 ECs among 400×400 (160,000) ECs for Schaefer 400-node parcellation (Schaefer et al., 2018). Given that all non-zero ECs had a Bayesian-PP exceeding 0.95, it follows that all these top one-half largest ECs also had Bayesian-PP values above 0.95.

3. Results

3.1. Sample characteristics

Out of the initial 40 participants who met the inclusion criteria, 6 were excluded: 1 because of left-handedness, 3 because of positive urine drug screens, 1 because of missing HRV data, and 1 because of missing necessary neuroimaging data (please refer to supplementary information Table 1 for specific exclusion details). Thus, a final analysis was conducted on 34 individuals. The 34 control participants included in these analyses had an average age of 32.68 ± 14.09 years (ranging from 18 to 68 years), with 19 identifying as biologically female and 15 as male. Approximately half of the sample identified as White ($n = 18$), while 12 participants identified as African American and 4 as Asian. On average, the participants had 15.88 years of education (standard deviation [SD] = 2.94 years) with a range of 12 to 25 years.

Table 1 contains a summary of statistics, including mean values and standard deviations of heart rate and HRV measures, and Pearson

Table 1

Correlations among HRV measures and heart rate, also showing means, standard deviations, and range.

	RMSSD	HF HRV	Heart rate (beats per minute)
Mean \pm SD	67.6 \pm 46.2	49.6 \pm 20.8	63.2 \pm 10.2
Range	(7.6 to 176.2)	(10.7 to 87.8)	(45.3 to 82.7)
HF HRV	$r = 0.62$ $p < 0.001$		
Heart rate (beats per minutes)	$r = -0.59$ $p < 0.001$	$r = -0.24$ $p = 0.18$	

Notes. SD= standard deviation; RMSSD= root mean square of successive differences; HF HRV= high-frequency heart rate variability.

correlation coefficients for these variables. There was a positive correlation between RMSSD and HF HRV ($r = 0.622, p = 0.0002$). Heart rate was negatively correlated with RMSSD ($r = -0.588, p = 0.0004$) but not with HF HRV ($r = -0.242, p > 0.05$).

3.2. Dynamic causal modeling results

3.2.1. Selection and localization of nodes for the primary spectral-DCM analysis

The exploratory regression-DCM analysis identified 12 nodes that were subsequently employed in the primary spectral-DCM analysis (for additional details, please refer to the supplementary information). These nodes included: left-VLPFC, right-VLPFC, mPFC, left-MTG, right-MTG, supracallosal (dorsal) ACC, right-insula, right-amygdala, right-hippocampus, left-thalamus, right-thalamus, and right-SMG. The same nodes were used for each participant. The amygdala, bilateral VLPFC, and ACC were among these 12 nodes predicted in Hypothesis 1.

3.3. Results of the primary spectral-DCM analyses

3.3.1. Results of the analysis testing if each effective connectivity (EC) was different from zero

At the group level, 83 connectivities had non-zero mean EC values with Bayesian-PP >0.95 . In Fig. 2, represented in the “Mean EC” panel, each of the 83 group-level mean ECs is depicted as a matrix element. For each matrix element, the source node of the EC is indicated by the node associated with the corresponding column label on the top x-axis, and the target node of the EC (i.e., the node of the EC which is influenced by the source node) is indicated by the corresponding row label on the left y-axis. To enhance clarity, we used numerical values within the matrix elements and a color code to emphasize the magnitude of ECs when the Bayesian-PP exceeds 0.95. In cases where the Bayesian-PP is less than or equal to 0.95, we represent the strength of the EC as zero, and display the color of the matrix element in white. The unit of each EC is hertz, which represents rate of change (Zeidman et al., 2019). Among the 83 non-zero ECs with PP >0.95 , the median of the absolute values of these ECs was 0.12 hertz. The strength of the EC from Region 1 to Region 2 is the rate of change in neural response in Region 2 due to neural activity in Region 1 (Zeidman et al., 2019). We designated the 41 ECs with absolute values surpassing this median as the top one-half largest ECs, as specified in the methods section. These top one-half largest absolute-value ECs were subsequently employed for testing the hypotheses described below.

3.3.2. Results of analyses testing the linear relationship between each EC, HRV, and heart rate

For each of the linear regression analyses, each of the 83 group-level linear regression coefficients (*beta*) is depicted as a matrix element, as shown in the panels in Fig. 2 for RMSSD *beta*, HF HRV *beta*, and heart

rate *beta*. Similar to the mean ECs, the value of each *beta* with a Bayesian-PP >0.95 is visually represented by a numerical value within each matrix element and a color code. In instances where the Bayesian-PP is less than or equal to 0.95, we represent the strength of the *beta* as zero, and display the color of the matrix element in white. Similar to the analysis testing if each EC magnitude was different from zero, the linear regression analyses were conducted for all the ECs. Frassle and Stephan (2022) found that resting-state fMRI test-retest reliability is robust for larger absolute-value EC magnitudes. Based on that work, a median-splitting threshold (0.12 hertz) was applied only to the EC magnitudes (measured in hertz) and not to the linear regression coefficients (*betas*). Note that the median-splitting threshold was only used for testing the hypotheses. Since this threshold was arbitrary, all the linear regression results, including those for the ECs whose absolute-value magnitudes did not surpass the threshold adopted in this study, are shown in Fig. 2.

3.4. Dynamic causal modeling (DCM) results for hypotheses 2A and 2B

Hypotheses 2A and 2B predicted that greater HRV would be associated with greater strength of ECs from the prefrontal regions to the amygdala, reflecting stronger top-down control, and that greater HRV would be associated with lower strength of ECs from the amygdala to the prefrontal regions, reflecting weaker bottom-up processing. Hypothesis 2A was not supported; we found that the mean values of ECs related to top-down processing, which encompassed the ECs from bilateral VLPFC, mPFC and ACC to the right amygdala, were all zero (Fig. 3). In contrast, results supported Hypothesis 2B, with three ECs consistent with bottom-up processing. Specifically, the strength of the ECs from the right amygdala to the ACC and to the bilateral VLPFC displayed a reliable negative linear relationship with both HRV measures, with the Bayesian-PP greater than 0.95 for the linear regression coefficient betas. The absolute values of these ECs ranked among the top one-half largest absolute values of ECs.

3.5. Dynamic causal modeling (DCM) results for hypothesis 3

Hypothesis 3 predicted that the ECs (not limited to only the top-down and/or bottom-up ECs) which displayed reliable linear relationships with HRV, would also demonstrate reliable inverse linear relationships with heart rate. Seven out of the 41 top one-half largest ECs showed reliable (Bayesian-PP >0.95) linear relationships with the two HRV measures (Fig. 4). These ECs included the three ECs from right amygdala to the ACC and to the bilateral VLPFC (shown in Fig. 3), the three ECs from left thalamus and bilateral MTG to the right VLPFC, and the EC from right MTG to the right insula. Consistent with our hypothesis, and as shown in Fig. 4, among these seven ECs, all (except the EC from right amygdala to the right VLPFC), showed a reliable positive linear relationship with heart rate, which was the opposite sign of their negative linear relationship with the HRV measures. The exception was the EC from right amygdala to the right VLPFC, which did not show a reliable positive or negative linear relationship with heart rate.

3.6. Results of the spectral-DCM analyses evaluating the effects of age, sex, education, and z-scoring

For each of the primary spectral-DCM analyses described above, we conducted a supplementary analysis that included age, sex, and education as covariates. Adding these covariates to our models did not markedly alter our initial results (see Supplementary Figure 3), with the findings related to the three ECs originating from the amygdala to the ACC and to the bilateral VLPFC preserved.

To evaluate further the effects of age, sex, and z-scoring of HRV and heart rate measures on results related to the ECs from the amygdala to the ACC and to the bilateral VLPFC, we conducted several additional supplementary DCM parametric empirical Bayes analyses. These

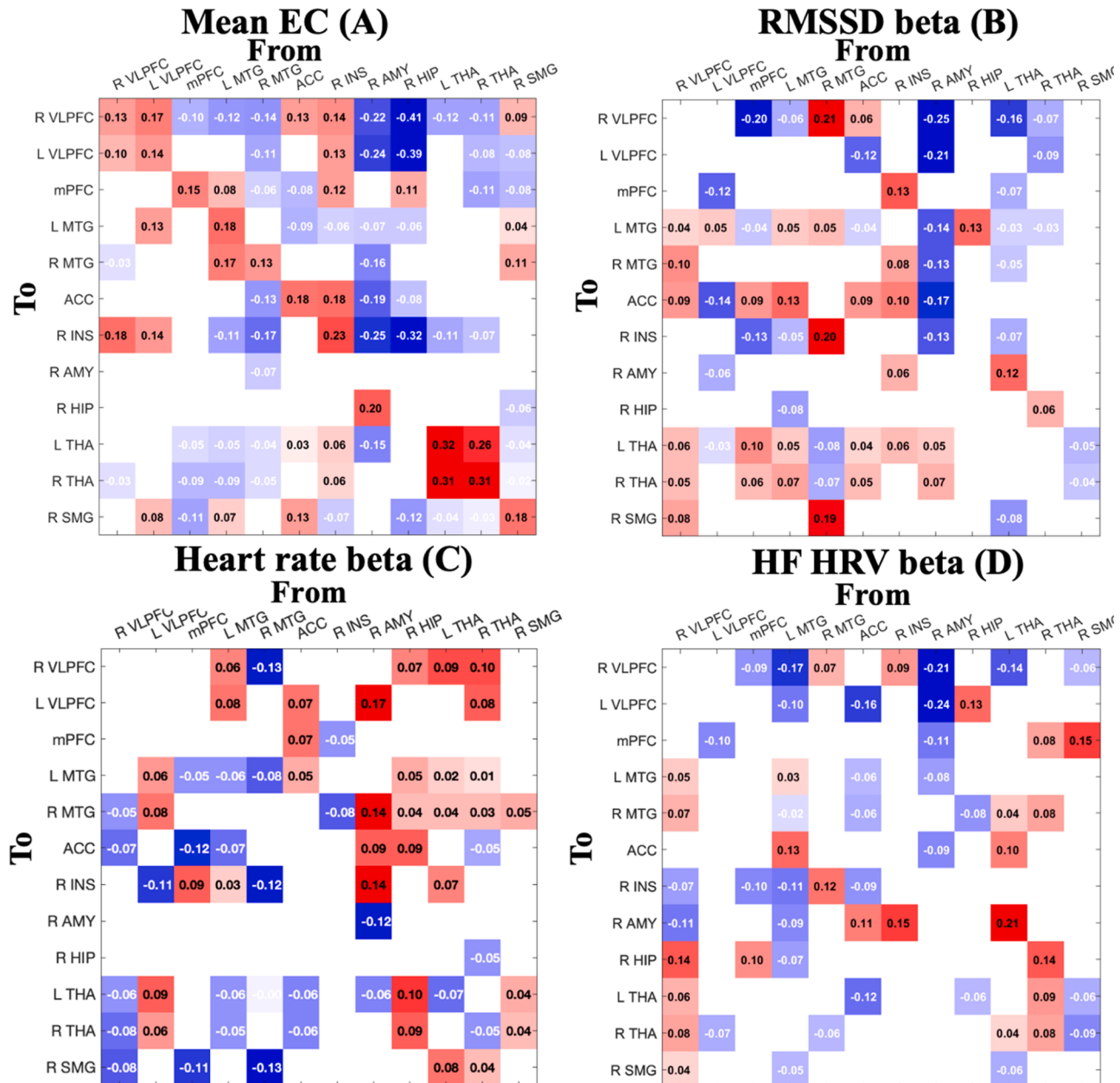


Fig. 2. Results of the primary Spectral-DCM analyses assessing if each EC (measured in hertz for off-diagonal ECs, and unitless for diagonal ECs) differs from zero, represented in the “Mean EC” matrix, and determining whether each linear regression coefficient (*beta*) (dimensionless) differs from zero, as indicated by the other four matrices, at the group level ($n = 34$ participants). Each beta matrix corresponds to the linear regression analysis between each EC and RMSSD, HF HRV, and heart rate. The magnitude of each EC (or *beta*) is illustrated by a matrix element, with the direction of the EC extending from the node denoted by the respective column label (located along the top x-axis) to the node identified by the corresponding row label (along the left y-axis). To facilitate demonstration, ECs (or *betas*) with Bayesian-PP equal to or below 0.95 are set to zero, indicated by a white matrix element. Non-zero ECs (or *betas*) with Bayesian-PP exceeding 0.95 are displayed through numerical values within the matrix cell and a color map. For each matrix element, a warmer color signifies that an EC (or *beta*) is greater than zero, while a cooler color indicates that an EC (or *beta*) is less than zero. Notes. ACC= anterior cingulate cortex, AMY= amygdala, HIP= hippocampus, INS= insula, mPFC= medial prefrontal cortex, MTG= middle temporal gyrus, SMG= supramarginal gyrus, THA= thalamus, VLPFC= ventrolateral prefrontal cortex).

additional supplementary analyses revealed that sex and z-scoring had no effects on the major findings (i.e., the ECs from the amygdala to the ACC and to the bilateral VLPFC). Greater amygdala to left VLPFC EC strength was associated with greater age. However, the amygdala to ACC EC and the amygdala to right VLPFC EC strengths did not covary with the age. See the Supplementary Information for the results of these additional analyses.

4. Discussion

In the present study, we performed DCM analyses on resting-state fMRI data to investigate relationships between ECs, HRV, and heart rate. Our selection of 12 DCM nodes was informed by prior research and the outcomes of an exploratory regression-DCM analysis that encompassed an extensive network throughout the entire brain. The primary DCM analyses indicated that ECs originating from the right amygdala to the ACC and to the bilateral VLPFC were among the most robust ECs, displaying reliable negative linear relationships with both HRV

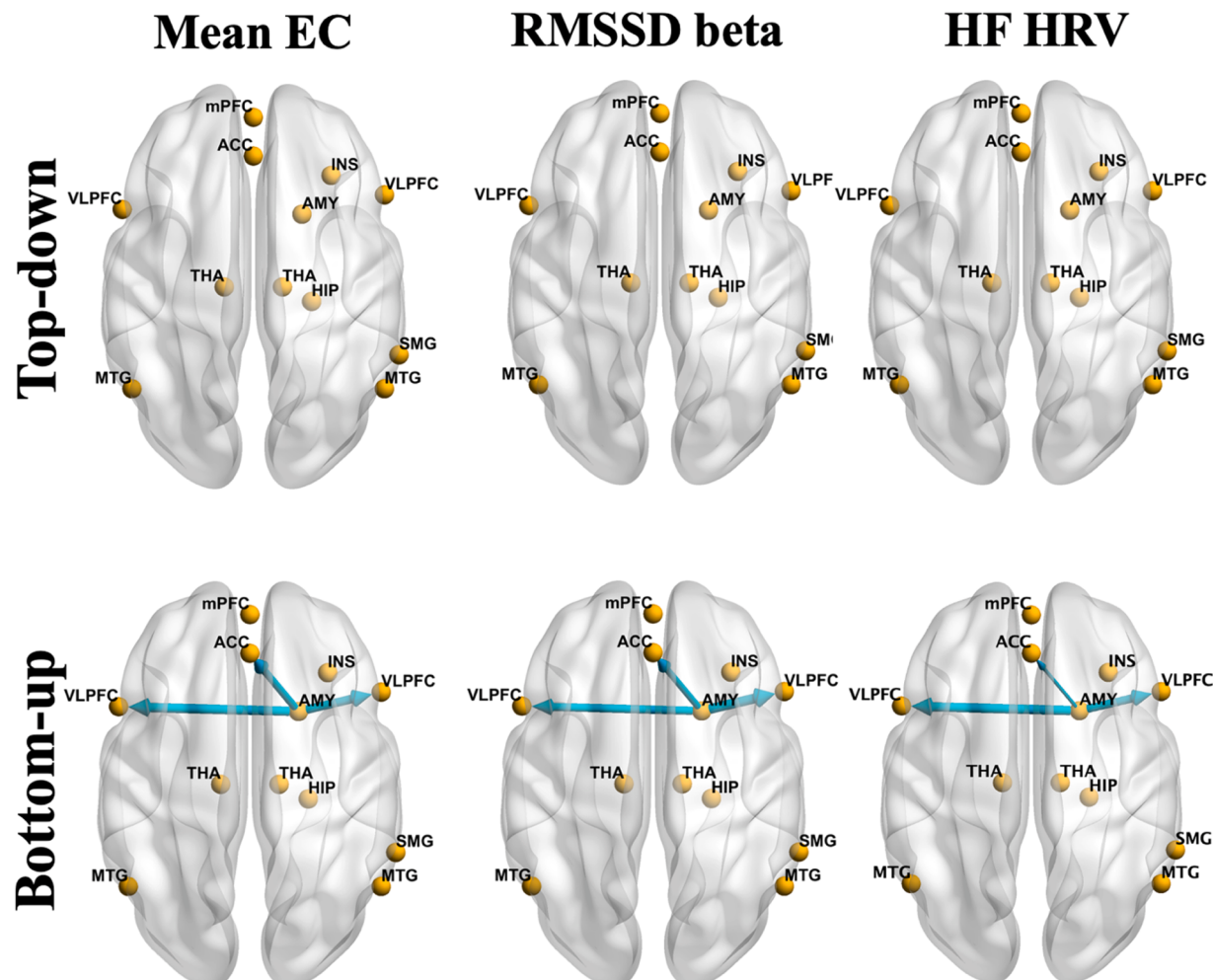


Fig. 3. Dynamic causal modelling (DCM) results related to Hypotheses 1A and 1B. The mean values of ECs related to top-down processing were all zero (upper panel). Three effective connectivities (ECs) related to bottom-up processing (lower panel) were among the top one-half largest ECs. These ECs displayed reliable linear relationship with RMSSD, HF HRV, and the stress index, with the Bayesian-PP exceeding 0.95 for the linear regression coefficient β . A red arrow line signifies a positive EC (or β), while a light blue line represents a negative EC (or β). The line width corresponds to the strength of the EC (or β). Abbreviations in the figure include ACC (anterior cingulate cortex), AMY (amygdala), HIP (hippocampus), INS (insula), mPFC (medial prefrontal cortex), MTG (middle temporal gyrus), SMG (supramarginal gyrus), THA (thalamus), and VLPFC (ventrolateral prefrontal cortex). The results were visualized using BrainNet Viewer (<http://www.nitrc.org/projects/bnv/>) (Xia et al., 2013). The viewer's left side corresponds to the brain's left hemisphere, while the right side represents the right hemisphere.

measures. The EC from the right amygdala to left VLPFC also exhibited a reliable positive linear relationship with heart rate. The DCM results, however, did not support our hypothesis 2A, as evidenced by ECs with zero values originating from the prefrontal regions to the amygdala.

The direct top-down regulation of prefrontal regions over limbic regions is typically associated with affect presentation and regulation (Etkin et al., 2011). Our results suggest that in healthy individuals during the resting state, this direct top-down regulation may not be prominently active. In contrast, the DCM results supported our hypothesis 2B regarding bottom-up processing. Specifically, the ECs from the right amygdala to the ACC and to the bilateral VLPFC exhibited substantial EC strength. These findings suggest that during the resting state, lower HRV is associated with greater bottom-up processing from the amygdala to prefrontal regions (ACC and VLPFC) in healthy individuals.

In a study relevant to ours, Sakaki et al. (2016) used fMRI-based resting-state functional connectivity and found that greater HRV was associated with stronger functional connectivity between the amygdala and the VLPFC in younger adults, but not in older adults. The authors also observed that greater HRV was associated with stronger functional connectivity between the right amygdala and the medial prefrontal

region (including the ACC) in both younger and older adults. Thus, the present study and Sakaki et al. (2016) both support the idea that prefrontal-amygdala circuits underlie HRV. However, it is important to note that while Sakaki et al. (2016) found a positive association between HRV and functional connectivity, our study found a negative association between HRV and EC. This difference may be attributed to the distinction between EC and functional connectivity. Theoretical considerations (Altman and Krzywinski, 2015) and experimental evidence (Saetia et al., 2020) suggest that EC can emerge between two brain regions independently of functional connectivity. As such, EC and functional connectivity should not be considered equivalent, regardless of the direction of EC (Chuang et al., 2023). Additionally, a recent study (Chuang et al., 2023) revealed that resting-state fMRI-based EC and functional connectivity may have different relationships with health-related measures.

We also observed that ECs from the right amygdala to the ACC and the bilateral VLPFC were all negative, whereas the ECs from the ACC and bilateral VLPFC to the right amygdala were all zero. These findings suggest that during resting state, when threat or salience is absent, the amygdala processes routine environmental or sensory information in a bottom-up manner. Within the context of bottom-up processing, the amygdala plays a key role in detecting changes in the body's internal

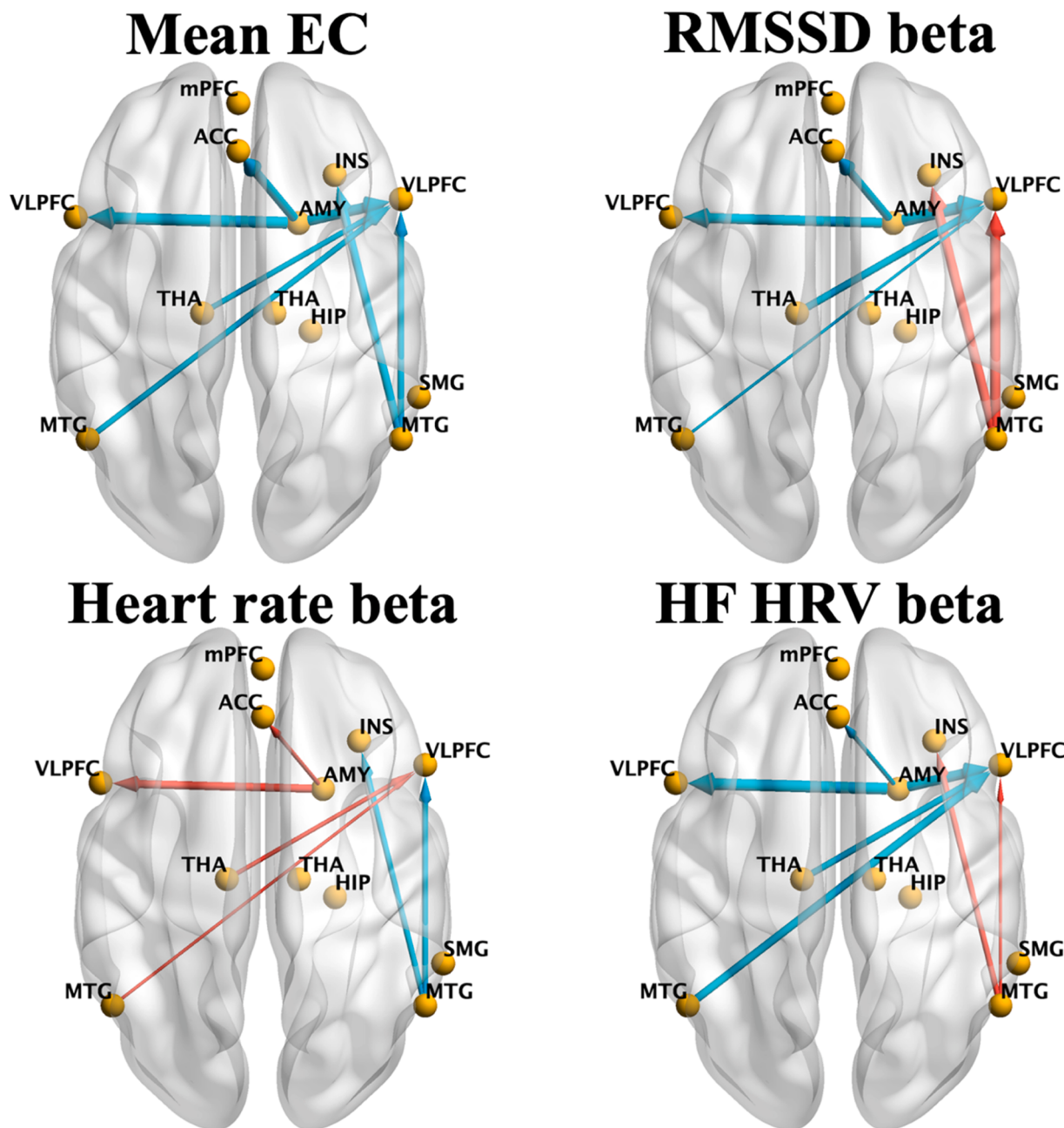


Fig. 4. Top one-half largest effective connectivities (ECs) which also show reliable linear relationship with the HRV measures and heart rate with a Bayesian-PP exceeding 0.95 for the linear regression coefficient *beta*. A red arrow line represents a positive EC (or *beta*), while a light blue line symbolizes a negative EC (or *beta*). Notes. ACC= anterior cingulate cortex, AMY= amygdala, HIP= hippocampus, INS= insula, mPFC= medial prefrontal cortex, MTG= middle temporal gyrus, SMG= supramarginal gyrus, THA= thalamus, VLPFC= ventrolateral prefrontal cortex). The viewer's left side corresponds to the brain's left hemisphere, while the right side represents the right hemisphere.

state, serving as an important center for interoception (Gothard and Fuglevand, 2022; Grundemann et al., 2019).

We found that the ECs from the right amygdala to the ACC and the bilateral VLPFC were all negative and that these ECs showed negative association with both HRV measures. Previous resting-state fMRI-based functional connectivity studies have investigated the prefrontal-amygdala circuits. Sripada et al. (2012) reported a negative correlation between the right amygdala and the dorsal ACC. Another study found that a greater change in functional connectivity between the amygdala and ACC is associated with a more pronounced autonomic response in fear conditioning (Schultz et al., 2012). Additionally, Fowler et al. (2017) found that greater functional connectivity between the bilateral amygdala and the right VLPFC is linked to both heightened

stress-reactive rumination and more pronounced depressive symptoms. These previous functional connectivity studies underscore the relevance and importance of the prefrontal-amygdala circuits and do not exclude the likelihood of our primary and novel EC findings, namely negative ECs from the amygdala to the ACC and bilateral VLPFC.

Our EC findings could also be interpreted based on prior animal studies and task-based human neuroimaging studies. In an animal study (Aggleton et al., 2015), projections from the amygdala to the prefrontal cortex were examined by injecting anterograde tracers into macaque monkeys. The study revealed that nearly all prefrontal areas (medial, orbital, and lateral regions) receive inputs from the amygdala. Based on existing literature, the authors of this study discussed the possibility that these amygdala-prefrontal projections may contribute to psychiatric

conditions such as anxiety disorders. In another animal study, using optogenetic strategies to activate or inhibit neurons in mice, Becker et al. (2023) manipulated ACC inputs from the basolateral amygdala and demonstrated that hyperactivity in the neuronal pathway connecting the basolateral amygdala to the ACC is critical for chronic pain-induced depression. A human study using magnetoencephalography-based DCM (Lu et al., 2012) found enhanced endogenous bottom-up EC from the amygdala to the ACC in patients with major depressive disorder compared to controls during a facial emotion processing task, and the authors suggested that the enhanced EC from the amygdala to the ACC may facilitate the ACC to monitor emotional challenges. In contrast, the present study, which involved healthy participants and did not include an emotional challenge, found negative (inhibitory) EC from the amygdala to the ACC.

Apart from the aforementioned three ECs extending from the amygdala to the prefrontal regions, four additional top one-half largest ECs exhibited reliable linear relationships with both the RMSSD HRV measure and the HF HRV measure. These four ECs were the three connections originating from the left thalamus and bilateral MTG to the right VLPFC, and the EC originating from the right MTG to the right insula. These results underscore the presence of brain regions (e.g., bilateral MTG) beyond those within the known CAN which may be associated with the neural mechanisms of HRV. The involvement of MTG is supported by previous studies (Duggento et al., 2016; Sakaki et al., 2016; Vanneste and De Ridder, 2013; Wei et al., 2018). While previous studies have identified a relationship between MTG and HRV, none have determined the potential role of MTG in influencing HRV. Further investigations are needed to explore and elucidate the potential contribution of MTG to HRV. Of the seven top one-half largest ECs exhibiting reliable linear relationships with the two HRV measures (i.e., the three ECs from right amygdala to the ACC and to the bilateral VLPFC, the three ECs from left thalamus and bilateral MTG to the right VLPFC, and the EC from right MTG to the right insula), six of these ECs also displayed a positive linear relationship with heart rate and thus with the opposite sign from the negative linear relationship of these ECs with the HRV measures. The only exception—the EC from right amygdala to the right VLPFC—exhibited a linear relationship with HRV but not heart rate. These findings highlight the intricate relationship between HRV and heart rate at the neural level, suggesting similarities or overlap of their underlying mechanisms. While we mainly discussed the direct connections between pairs of brain regions, it is necessary to note that in the context of EC, the causal influence which one node exerts over another can also be indirect, passing through a third node (Colombo and Weinberger, 2018). For example, the causal influence which the right VLPFC exerts over the amygdala may occur through the right MTG, with an EC of -0.03 Hz from right VLPFC to right MTG, and an EC of -0.07 Hz from right MTG to right amygdala (Fig. 2a).

The identification of integrated neural and cardiovascular system processes may also present opportunities for clinical intervention (Bates et al., 2023), with the present study's findings having potential implications for mind-body therapies, particularly the results related to ECs between the amygdala and prefrontal regions. Previous studies have shown that the circuits between the ACC and amygdala can be altered by intervention or disease. For example, the resting-state functional connectivity between the amygdala and dorsal prefrontal cortex was enhanced after Pavlovian fear conditioning (Schultz et al., 2012), and individuals with post-traumatic stress disorder exhibited a reduced negative correlation between the amygdala and the ACC (Sripada et al., 2012). Conversely, mindfulness practices have been shown to increase HRV (Kirk and Axelsen, 2020), while also decreasing amygdala activation (Kral et al., 2018) and increasing functional connectivity between the amygdala and the prefrontal regions (Taren et al., 2015). Additionally, neurofeedback training increased functional connectivity between the amygdala and the VLPFC (Young et al., 2018), and daily biofeedback increased resting-state functional connectivity between the amygdala and the medial prefrontal cortex (Nashiro et al., 2023).

Building on these prior studies, our DCM results suggest that the EC pathways from the amygdala to prefrontal regions might serve as potential neural targets for intervention studies aimed at improving HRV. Interventions could include approaches such as HRV biofeedback (Lehrer et al., 2000; Schumann et al., 2021). At the same time, it is essential to acknowledge differences in findings between our study and previous ones. For instance, there are differences in the specific prefrontal regions implicated in the regulation of resting-state HRV (ACC and VLPFC in our study versus the more general dorsal prefrontal cortex (Schultz et al., 2012), medial prefrontal cortex (Nashiro et al., 2023), or overall prefrontal regions (Taren et al., 2015) in previous studies.

Although this study had numerous strengths including the use of novel EC methodologies, regression DCM, and ICA, some important limitations should be noted. 1) Our spectral-DCM analysis was based on a relatively small 12-node network. Consequently, we may have missed relevant ECs involving brain regions that could be involved in the regulation of HRV and heart rate. For example, in Step 1 (exploratory analysis of large network EC using regression-DCM), the bilateral locus coeruleus (a region which was recently shown to be relevant to HRV) (Bachman et al., 2023), was excluded from the analysis due to its relatively small size. Further, the left insula, left amygdala, and major nodes of the default mode network, such as posterior cingulate cortex and angular gyrus, which are associated with HRV and blood pressure (Matusik et al., 2023; Min et al., 2024; Mohanta et al., 2023) were excluded from the present study because of not meeting our brain region selection criteria. The decision to keep the network small was primarily due to practical considerations because expanding the network size significantly increases the time required for DCM analysis (Seghier and Friston, 2013). However, it is important to highlight that these 12 DCM nodes were chosen based on their strong likelihood of being related to HRV, drawing from both existing literature and the results of the exploratory regression-DCM analysis conducted within a more extensive whole-brain network. 2) Our sample size of 34 participants is relatively small given the need to maximize resting-state fMRI data reliability. Our recent empirical study (Ma et al., 2024) demonstrated that DCM sample sizes of $n = 30$, $n = 35$, and $n = 40$ subjects had approximately 85 %, 87.5 %, and 90 % capability, respectively, to replicate the DCM outcomes observed in a larger sample ($n = 160$). Therefore, our sample size of $n = 34$ likely had approximately 87.5 % capability to replicate the major ECs related to HRV and heart rate relative to a sample size of $n = 160$. In the present study, out of the original 40 participants, 6 (15 %) had been excluded prior to data analysis. The exclusion of six participants did not markedly affect the reliability of the DCM results (approximately 87.5 % capability to replicate $n = 160$ when $n = 34$, versus 90 % capability when $n = 40$) (Ma et al., 2024). 3) In this study, we did not collect data specifically related to respiration. Although respiratory rate can be indirectly estimated from photoplethysmography data using frequency-based techniques and time domain detection (Chin et al., 2024; Kontaxis et al., 2020), we elected not to include respiratory rate estimations in our models to avoid problems of multicollinearity. 4) Participants spanned a wide range of ages. To assess the effect of age, we conducted two supplementary analyses. The first supplementary analysis demonstrated that the findings from our primary DCM analysis (i.e., the spectral-DCM analysis) remained consistent even when age was entered into the statistical model as a covariate. In the second supplementary analysis, which directly examined the relationship between ECs and age, we observed a positive association between age and the EC from amygdala to the left VLPFC. However, the ECs from the amygdala to the ACC and the right VLPFC did not show significant covariance with age. Further research should explore the influence of age in more depth.

To summarize, the selection of DCM nodes in this study was based on their strong likelihood of being related to HRV, informed by a combination of existing knowledge and the outcomes of our exploratory regression-DCM analysis encompassing a comprehensive network throughout the entire brain. The DCM analyses revealed that ECs from the right amygdala to the ACC and to the VLPFC displayed a negative

linear relationship with HRV, while exhibiting a positive linear relationship with heart rate. These findings of directional connections from the amygdala to the prefrontal regions contribute to the specificity of current theoretical models and if replicated, may offer potential neural targets for intervention studies aiming to enhance HRV. Supplementary analyses indicated that the primary findings were unlikely to be influenced significantly by demographic factors.

Data and code availability statements

A MATLAB implementation of the spectral dynamic causal modeling approach is available as open-source code in the Statistical Parametric Mapping software package (<https://www.fil.ion.ucl.ac.uk/spm/>). A MATLAB implementation of the regression dynamic causal modeling approach is available as open-source code in the Translational Algorithms for Psychiatry-Advancing Science (TAPAS) software package (<https://www.translationalneuromodeling.org/tapas>). The data used in this study is not able to be made openly available because of or restrictions related to ethics or privacy imposed by the local administering institution.

Disclosures

David Eddie is on the scientific advisory boards of mental-healthcare companies ViviHealth and Innerworld and is a partner in Peer Recovery Consultants. The remaining authors declare that they have no known potential competing financial or personal interests.

CRediT authorship contribution statement

Liangsuo Ma: Writing – review & editing, Writing – original draft, Visualization, Validation, Software, Methodology, Investigation, Formal analysis, Data curation, Conceptualization. **Larry D. Keen:** Writing – review & editing, Software, Methodology, Investigation, Formal analysis, Conceptualization. **Joel L. Steinberg:** Writing – review & editing, Resources, Methodology, Investigation, Data curation. **David Eddie:** Writing – review & editing. **Alex Tan:** Writing – review & editing. **Lori Keyser-Marcus:** Writing – review & editing, Project administration, Investigation. **Antonio Abbate:** Writing – review & editing. **F. Gerard Moeller:** Writing – review & editing, Validation, Supervision, Resources, Project administration, Methodology, Investigation, Funding acquisition, Conceptualization.

Declaration of competing interest

None.

Data availability

The data that has been used is confidential.

Acknowledgments

This research received support from the NIH HEAL Initiative under award number U54DA038999, the Medication Development Center for Cocaine Use Disorder, with Dr. F. Gerard Moeller as the Principal Investigator. Dr. Larry Keen II was supported by a Research Enhancement Award (1R15 DA052886-01A1) from the National Institute on Drug Abuse. Dr. David Eddie received funding from the National Institute on Alcohol Abuse and Alcoholism through awards K23AA027577-01A1 and L30AA026135-02. The views expressed in this work are solely those of the authors and do not necessarily reflect the official views of the National Center for Advancing Translational Sciences or the National Institutes of Health.

Supplementary materials

Supplementary material associated with this article can be found, in the online version, at doi:[10.1016/j.neuroimage.2024.120869](https://doi.org/10.1016/j.neuroimage.2024.120869).

References

- Aggleton, J.P., Wright, N.F., Rosene, D.L., Saunders, R.C., 2015. Complementary patterns of direct amygdala and hippocampal projections to the macaque prefrontal cortex. *Cereb. Cortex.* 25, 4351–4373.
- Altman, N., Krzywinski, M., 2015. Association, correlation and causation. *Nat. Methods* 12, 899–900.
- Appelhans, B.M., Luecken, L.J., 2006. Heart rate variability as an index of regulated emotional responding. *Rev. General Psychol.* 10, 229–240.
- Arnsten, A.F., 2009. Stress signalling pathways that impair prefrontal cortex structure and function. *Nat. Rev. Neurosci.* 10, 410–422.
- Bachman, S.L., Cole, S., Yoo, H.J., Nashiro, K., Min, J., Mercer, N., Nasseri, P., Thayer, J. F., Lehrer, P., Mather, M., 2023. Daily heart rate variability biofeedback training decreases locus coeruleus MRI contrast in younger adults in a randomized clinical trial. *Int. J. Psychophysiol.* 193, 112241.
- Baig, S.A., 2020. Bayesian inference: an introduction to hypothesis testing using bayes factors. *Nicotine Tob. Res.* 22, 1244–1246.
- Barbas, H., Zikopoulos, B., 2007. The prefrontal cortex and flexible behavior. *Neuroscientist.* 13, 532–545.
- Bastos, A.M., Usey, W.M., Adams, R.A., Mangun, G.R., Fries, P., Friston, K.J., 2012. Canonical microcircuits for predictive coding. *Neuron* 76, 695–711.
- Bates, M.E., Eddie, D., Lehrer, P.M., Nolan, R.P., Siepmann, M., 2023. Editorial: integrated cardiovascular and neural system processes as potential mechanisms of behavior change. *Front. Psychiatry* 14, 1175691.
- Becker, L.J., Fillinger, C., Waegaert, R., Journee, S.H., Hener, P., Ayazgok, B., Humo, M., Karatas, M., Thouayre, M., Gaikwad, M., Degiorgis, L., Santin, M.D.N., Mondino, M., Barrot, M., Ibrahim, E.C., Turecki, G., Belzeaux, R., Veinante, P., Harsan, L.A., Hugel, S., Lutz, P.E., Yalcin, I., 2023. The basolateral amygdala-anterior cingulate pathway contributes to depression-like behaviors and comorbidity with chronic pain behaviors in male mice. *Nat. Commun.* 14, 2198.
- Behzadi, Y., Restom, K., Liu, J., Liu, T.T., 2007. A component based noise correction method (CompCor) for BOLD and perfusion based fMRI. *Neuroimage* 37, 90–101.
- Beissner, F., Meissner, K., Bar, K.J., Napadow, V., 2013. The autonomic brain: an activation likelihood estimation meta-analysis for central processing of autonomic function. *J. Neurosci.* 33, 10503–10511.
- Benarroch, E.E., 1993. The central autonomic network: functional organization, dysfunction, and perspective. *Mayo Clin. Proc.* 68, 988–1001.
- Benarroch, E.E., 1997. The central autonomic network. In: Low, P.A. (Ed.), *Clinical Autonomic Disorders*. Lippincott-Raven, Philadelphia, pp. 17–23.
- Calhoun, V.D., Adali, T., Pearson, G.D., Pekar, J.J., 2001. Spatial and temporal independent component analysis of functional MRI data containing a pair of task-related waveforms. *Hum. Brain Mapp.* 13, 43–53.
- Calhoun, V.D., de Lacy, N., 2017. Ten key observations on the analysis of resting-state functional MR imaging data using independent component analysis. *Neuroimaging Clin. N. Am.* 27, 561–579.
- Chand, T., Li, M., Jamalabadi, H., Wagner, G., Lord, A., Alizadeh, S., Danyeli, L.V., Herrmann, L., Walter, M., Sen, Z.D., 2020. Heart rate variability as an index of differential brain dynamics at rest and after acute stress induction. *Front. Neurosci.* 14, 645.
- Chang, C., Metzger, C.D., Glover, G.H., Duyn, J.H., Heinze, H.J., Walter, M., 2013. Association between heart rate variability and fluctuations in resting-state functional connectivity. *Neuroimage* 68, 93–104.
- Chen, C.H., Suckling, J., Ooi, C., Fu, C.H., Williams, S.C., Walsh, N.D., Mitterschiffthaler, M.T., Pich, E.M., Bullmore, E., 2008. Functional coupling of the amygdala in depressed patients treated with antidepressant medication. *Neuropsychopharmacology* 33, 1909–1918.
- Chin, W.J., Kwan, B.H., Lim, W.Y., Tee, Y.K., Darmaraju, S., Liu, H., Goh, C.H., 2024. A novel respiratory rate estimation algorithm from photoplethysmogram using deep learning model. *Diagnostics. (Basel)* 14.
- Chuang, K.C., Ramakrishnapillai, S., Madden, K., St Amant, J., McKIveen, K., Gwizdala, K., Dhullipudi, R., Bazzano, L., Carmichael, O., 2023. Brain effective connectivity and functional connectivity as markers of lifespan vascular exposures in middle-aged adults: the Bogalusa Heart Study. *Front. Aging Neurosci.* 15, 1110434.
- Colombo, M., Weinberger, N., 2018. Discovering brain mechanisms using network analysis and causal modeling. *Minds Mach. (Dordr.)* 28, 265–286. <https://doi.org/10.1007/s11023-017-9447-0>.
- Cox, R.W., 1996. AFNI: software for analysis and visualization of functional magnetic resonance neuroimages. *Comput. Biomed. Res.* 29, 162–173.
- Crutchley, H.D., 2005. Neural mechanisms of autonomic, affective, and cognitive integration. *J. Comp. Neurol.* 493, 154–166.
- Crutchley, H.D., 2009. Psychophysiology of neural, cognitive and affective integration: fMRI and autonomic indicants. *Int. J. Psychophysiol.* 73, 88–94.
- Duggento, A., Bianciardi, M., Passamonti, L., Wald, L.L., Guerrisi, M., Barbieri, R., Toschi, N., 2016. Globally conditioned Granger causality in brain-brain and brain-heart interactions: a combined heart rate variability/ultra-high-field (7 T) functional magnetic resonance imaging study. *Philos. Trans. a Math. Phys. Eng. Sci.* 374.
- Etkin, A., Egner, T., Kalisch, R., 2011. Emotional processing in anterior cingulate and medial prefrontal cortex. *Trends. Cogn. Sci.* 15, 85–93.

- Everitt, B.J., Cardinal, R.N., Hall, J., Parkinson, J., Robbins, T., 2000. Differential involvement of amygdala subsystems in appetitive conditioning and drug addiction. *amygdala: Functional Anal.* 353–390.
- Fowler, C.H., Miernicki, M.E., Rudolph, K.D., Telzer, E.H., 2017. Disrupted amygdala-prefrontal connectivity during emotion regulation links stress-reactive rumination and adolescent depressive symptoms. *Dev. Cogn. Neurosci.* 27, 99–106.
- Frassle, S., Aponte, E.A., Bollmann, S., Brodersen, K.H., Do, C.T., Harrison, O.K., Harrison, S.J., Heinze, J., Iglesias, S., Kasper, L., Lomakina, E.I., Mathys, C., Muller-Schrader, M., Pereira, I., Petzschner, F.H., Raman, S., Schobi, D., Toussaint, B., Weber, L.A., Yao, Y., Stephan, K.E., 2021a. TAPAS: an open-source software package for translational neuromodeling and computational psychiatry. *Front. Psychiatry* 12, 680811.
- Frassle, S., Harrison, S.J., Heinze, J., Clementz, B.A., Tamminga, C.A., Sweeney, J.A., Gershon, E.S., Keshavan, M.S., Pearlson, G.D., Powers, A., Stephan, K.E., 2020. Regression dynamic causal modeling for resting-state fMRI. *bioRxiv*. <https://doi.org/10.1101/2020.08.12.247536>.
- Frassle, S., Lomakina, E.I., Kasper, L., Manjaly, Z.M., Leff, A., Pruessmann, K.P., Buhmann, J.M., Stephan, K.E., 2018. A generative model of whole-brain effective connectivity. *Neuroimage* 179, 505–529.
- Frassle, S., Lomakina, E.I., Razi, A., Friston, K.J., Buhmann, J.M., Stephan, K.E., 2017. Regression DCM for fMRI. *Neuroimage* 155, 406–421.
- Frassle, S., Manjaly, Z.M., Do, C.T., Kasper, L., Pruessmann, K.P., Stephan, K.E., 2021b. Whole-brain estimates of directed connectivity for human connectomics. *Neuroimage* 225, 117491.
- Frassle, S., Stephan, K.E., 2022. Test-retest reliability of regression dynamic causal modeling. *Netw. Neurosci.* 6, 135–160.
- Friston, K.J., 2011. Functional and effective connectivity: a review. *Brain Connect.* 1, 13–36. PMID: 22432952.
- Friston, K.J., Harrison, L., Penny, W., 2003. Dynamic causal modelling. *Neuroimage* 19, 1273–1302. PMID: 12948688.
- Friston, K.J., Kahan, J., Biswal, B., Razi, A., 2014. A DCM for resting state fMRI. *Neuroimage* 94, 396–407.
- Friston, K.J., Li, B., Daunizeau, J., Stephan, K.E., 2011. Network discovery with DCM. *Neuroimage* 56, 1202–1221. PMID: 21182971.
- Friston, K.J., Litvak, V., Oswal, A., Razi, A., Stephan, K.E., van Wijk, B.C., Ziegler, G., Zeidman, P., 2016. Bayesian model reduction and empirical Bayes for group (DCM) studies. *Neuroimage* 128, 413–431.
- Friston, K.J., Penny, W., 2003. Posterior probability maps and SPMs. *Neuroimage* 19, 1240–1249.
- Friston, K.J., Penny, W., 2011. Post hoc Bayesian model selection. *Neuroimage* 56, 2089–2099.
- Friston, K.J., Preller, K.H., Mathys, C., Cagnan, H., Heinze, J., Razi, A., Zeidman, P., 2019. Dynamic causal modelling revisited. *Neuroimage* 199, 730–744.
- Gabbott, P.L., Warner, T.A., Busby, S.J., 2006. Amygdala input monosynaptically innervates parvalbumin immunoreactive local circuit neurons in rat medial prefrontal cortex. *Neuroscience* 139, 1039–1048.
- Glasser, M.F., Coalson, T.S., Robinson, E.C., Hacker, C.D., Harwell, J., Yacoub, E., Ugurbil, K., Andersson, J., Beckmann, C.F., Jenkinson, M., Smith, S.M., Van Essen, D.C., 2016. A multi-modal parcellation of human cerebral cortex. *Nature* 536, 171–178.
- Goldstein, D.S., 2001. *The Autonomic Nervous System in Health and Disease*. NY: Marcel Dekker, Inc., New York.
- Gothard, K.M., Fuglevand, A.J., 2022. The role of the amygdala in processing social and affective touch. *Curr. Opin. Behav. Sci.* 43, 46–53.
- Grundemann, J., Bitterman, Y., Lu, T., Krabbe, S., Grewe, B.F., Schnitzer, M.J., Luthi, A., 2019. Amygdala ensembles encode behavioral states. *Science (1979)* 364.
- He, Z., 2020. The control mechanisms of heart rate dynamics in a new heart rate nonlinear time series model. *Sci. Rep.* 10, 4814.
- Hyravinen, A., 2013. Independent component analysis: recent advances. *Philos. Trans. a Math. Phys. Eng. Sci.* 371, 20110534.
- Jenkinson, M., Bannister, P., Brady, M., Smith, S., 2002. Improved optimization for the robust and accurate linear registration and motion correction of brain images. *Neuroimage* 17, 825–841.
- Kasper, L., Bollmann, S., Diaconescu, A.O., Hutton, C., Heinze, J., Iglesias, S., Hauser, T.U., Sebold, M., Manjaly, Z.M., Pruessmann, K.P., Stephan, K.E., 2017. The PhysIO toolbox for modeling physiological noise in fMRI data. *J. Neurosci. Methods* 276, 56–72.
- Kazmi, S.Z., Zhang, H., Aziz, W., Monfredi, O., Abbas, S.A., Shah, S.A., Kazmi, S.S., Butt, W.H., 2016. Inverse correlation between heart rate variability and heart rate demonstrated by linear and nonlinear analysis. *PLoS. One* 11, e0157557.
- Keyser-Marcus, L.A., Ramey, T., Bjork, J., Adams, A., Moeller, F.G., 2021. Development and feasibility study of an addiction-focused phenotyping assessment battery. *Am. J. Addict.* 30, 398–405.
- Kim, H.G., Cheon, E.J., Bai, D.S., Lee, Y.H., Koo, B.H., 2018. Stress and heart rate variability: a meta-analysis and review of the literature. *Psychiatry Investig.* 15, 235–245.
- Kirk, U., Axelsen, J.L., 2020. Heart rate variability is enhanced during mindfulness practice: a randomized controlled trial involving a 10-day online-based mindfulness intervention. *PLoS. One* 15, e0243488.
- Kontaxis, S., Lazaro, J., Corino, V.D.A., Sandberg, F., Bailon, R., Laguna, P., Sornmo, L., 2020. ECG-derived respiratory rate in atrial fibrillation. *IEEE Trans. Biomed. Eng.* 67, 905–914.
- Kral, T.R.A., Schuyler, B.S., Mumford, J.A., Rosenkranz, M.A., Lutz, A., Davidson, R.J., 2018. Impact of short- and long-term mindfulness meditation training on amygdala reactivity to emotional stimuli. *Neuroimage* 181, 301–313.
- Kujawa, A., Wu, M., Klumpp, H., Pine, D.S., Swain, J.E., Fitzgerald, K.D., Monk, C.S., Phan, K.L., 2016. Altered development of amygdala-anterior cingulate cortex connectivity in anxious youth and young adults. *Biol. Psychiatry Cogn. Neurosci. Neuroimaging* 1, 345–352.
- Laborde, S., Mosley, E., Thayer, J.F., 2017. Heart rate variability and cardiac vagal tone in psychophysiological research - recommendations for experiment planning, data analysis, and data reporting. *Front. Psychol.* 8, 213.
- Lane, R.D., McRae, K., Reiman, E.M., Chen, K., Ahern, G.L., Thayer, J.F., 2009. Neural correlates of heart rate variability during emotion. *Neuroimage* 44, 213–222.
- LeDuke, D.O., Borio, M., Miranda, R., Tye, K.M., 2023. Anxiety and depression: a top-down, bottom-up model of circuit function. *Ann. N. Y. Acad. Sci.* 1525, 70–87.
- Lee, D., Park, J., Namkoong, K., Hong, S.J., Kim, I.Y., Jung, Y.C., 2020. Diminished cognitive control in Internet gaming disorder: a multimodal approach with magnetic resonance imaging and real-time heart rate variability. *Prog. Neuropsychopharmacol. Biol. Psychiatry* 111, 110127.
- Lee, D., Park, J., Namkoong, K., Hong, S.J., Kim, I.Y., Jung, Y.C., 2021. Diminished cognitive control in Internet gaming disorder: a multimodal approach with magnetic resonance imaging and real-time heart rate variability. *Prog. Neuropsychopharmacol. Biol. Psychiatry* 111, 110127.
- Lehrer, P.M., Vaschillo, E., Vaschillo, B., 2000. Resonant frequency biofeedback training to increase cardiac variability: rationale and manual for training. *Appl. Psychophysiol. Biofeedback.* 25, 177–191.
- Lu, Q., Li, H., Luo, G., Wang, Y., Tang, H., Han, L., Yao, Z., 2012. Impaired prefrontal-amygdala effective connectivity is responsible for the dysfunction of emotion process in major depressive disorder: a dynamic causal modeling study on MEG. *Neurosci. Lett.* 523, 125–130.
- Ma, L., Braun, S.E., Steinberg, J.L., Bjork, J.M., Martin, C.E., Keen 2nd, L.D., Moeller, F.G., 2024. Effect of scanning duration and sample size on reliability in resting state fMRI dynamic causal modeling analysis. *Neuroimage*, 120604.
- Ma, L., Hettema, J.M., Cousijn, J., Bjork, J.M., Steinberg, J.L., Keyser-Marcus, L., Woisard, K., Lu, Q., Roberson-Nay, R., Abbate, A., Moeller, F.G., 2021. Resting-state directional connectivity and anxiety and depression symptoms in adult cannabis users. *Biol. Psychiatry Cogn. Neurosci. Neuroimaging* 6, 545–555.
- Malik, M., Bigger, J.T., Camm, A.J., Kleiger, R.E., Malliani, A., Moss, A.J., Schwartz, P.J., 1996. Heart rate variability: standards of measurement, physiological interpretation, and clinical use. task force of the european society of cardiology and the north american society of pacing and electrophysiology. *Eur. Heart. J.* 17, 354–381.
- Matusik, P.S., Zhong, C., Matusik, P.T., Alomar, O., Stein, P.K., 2023. Neuroimaging studies of the neural correlates of heart rate variability: a systematic review. *J. Clin. Med.* 12.
- Mayhugh, R.E., Laurienti, P.J., Fanning, J., Gauvin, L., Heilman, K.J., Porges, S.W., Rejeski, W.J., 2018. Cardiac vagal dysfunction moderates patterns of craving across the day in moderate to heavy consumers of alcohol. *PLoS. One* 13, e0200424.
- McKeown, M.J., Makeig, S., Brown, G.G., Jung, T.P., Kindermann, S.S., Bell, A.J., Sejnowski, T.J., 1998. Analysis of fMRI data by blind separation into independent spatial components. *Hum Brain Mapp* 6, 160–188.
- Menon, V., Uddin, L.Q., 2010. Saliency, switching, attention and control: a network model of insula function. *Brain Struct. Funct.* 214, 655–667.
- Min, J., Koenig, J., Nashiro, K., Yoo, H.J., Cho, C., Thayer, J.F., Mather, M., 2024. Resting heart rate variability is associated with neural adaptation when repeatedly exposed to emotional stimuli. *Neuropsychologia* 196, 108819.
- Mohanta, S.K., Yin, C., Weber, C., Godinho-Silva, C., Veiga-Fernandes, H., Xu, Q.J., Chang, R.B., Habenicht, A.J.R., 2023. Cardiovascular brain circuits. *Circ. Res.* 132, 1546–1565.
- Monfredi, O., Lyashkov, A.E., Johnsen, A.B., Inada, S., Schneider, H., Wang, R., Nirmalan, M., Wisloff, U., Maltsev, V.A., Lakatta, E.G., Zhang, H., Boyett, M.R., 2014. Biophysical characterization of the underappreciated and important relationship between heart rate variability and heart rate. *Hypertension* 64, 1334–1343.
- Nashiro, K., Min, J., Yoo, H.J., Cho, C., Bachman, S.L., Dutt, S., Thayer, J.F., Lehrer, P.M., Feng, T., Mercer, N., Nasser, P., Wang, D., Chang, C., Marmarelis, V.Z., Narayanan, S., Nation, D.A., Mather, M., 2023. Increasing coordination and responsiveness of emotion-related brain regions with a heart rate variability biofeedback randomized trial. *Cogn. Affect. Behav. Neurosci.* 23, 66–83.
- Nikolin, S., Boonstra, T.W., Loo, C.K., Martin, D., 2017. Combined effect of prefrontal transcranial direct current stimulation and a working memory task on heart rate variability. *PLoS. One* 12, e0181833.
- Novelli, L., Friston, K., Razi, A., 2024. Spectral dynamic causal modeling: a didactic introduction and its relationship with functional connectivity. *Network Neurosci.* 8, 178–202.
- Parkes, L., Fulcher, B., Yucl, M., Fornito, A., 2018. An evaluation of the efficacy, reliability, and sensitivity of motion correction strategies for resting-state functional MRI. *Neuroimage* 171, 415–436.
- Penny, W.D., Stephan, K.E., Daunizeau, J., Rosa, M.J., Friston, K.J., Schofield, T.M., Leff, A.P., 2010. Comparing families of dynamic causal models. *PLoS. Comput. Biol.* 6, e1000709. PMID: 20300649.
- Pham, T., Lau, Z.J., Chen, S.H.A., Makowski, D., 2021. Heart rate variability in psychology: a review of HRV indices and an analysis tutorial. *Sensors. (Basel)* 21.
- Pruim, R.H.R., Mennes, M., Buitelaar, J.K., Beckmann, C.F., 2015a. Evaluation of ICA-AROMA and alternative strategies for motion artifact removal in resting state fMRI. *Neuroimage* 112, 278–287.
- Pruim, R.H.R., Mennes, M., van Rooij, D., Llera, A., Buitelaar, J.K., Beckmann, C.F., 2015b. ICA-AROMA: a robust ICA-based strategy for removing motion artifacts from fMRI data. *Neuroimage* 112, 267–277.

- Razi, A., Seghier, M.L., Zhou, Y., McColgan, P., Zeidman, P., Park, H.-J., Sporns, O., Rees, G., Friston, K.J., 2017. Large-scale DCMs for resting-state fMRI. *Network Neurosci.* 1, 222–241.
- Rickham, P.P., 1964. Human experimentation. *Code of ethics of the world medical association. Declaration of helsinki.* Br. Med. J. 2, 177.
- Rolls, E.T., Huang, C.C., Lin, C.P., Feng, J., Joliot, M., 2020. Automated anatomical labelling atlas 3. *Neuroimage* 206, 116189.
- Saetia, S., Rosas, F., Ogata, Y., Yoshimura, N., Yasuharu, K., 2020. Comparison of resting-state functional and effective connectivity between default mode network and memory encoding related areas. *J. Neurosci. Neurol. Disorders* 4, 029–037.
- Sakaki, M., Yoo, H.J., Nga, L., Lee, T.H., Thayer, J.F., Mather, M., 2016. Heart rate variability is associated with amygdala functional connectivity with MPFC across younger and older adults. *Neuroimage* 139, 44–52.
- Schaefer, A., Kong, R., Gordon, E.M., Laumann, T.O., Zuo, X.N., Holmes, A.J., Eickhoff, S.B., Yeo, B.T.T., 2018. Local-Global Parcellation of the Human Cerebral Cortex from Intrinsic Functional Connectivity MRI. *Cereb Cortex* 28, 3095–3114.
- Schielzeth, H., 2010. Simple means to improve the interpretability of regression coefficients. *Methods Ecol. Evol.* 1, 103–113.
- Schultz, D.H., Balderston, N.L., Helmstetter, F.J., 2012. Resting-state connectivity of the amygdala is altered following Pavlovian fear conditioning. *Front. Hum. Neurosci.* 6, 242.
- Schumann, A., de la Cruz, F., Köhler, S., Brotte, L., Bär, K.-J., 2020. The influence of heart rate variability biofeedback on cardiac regulation and functional brain connectivity. *bioRxiv preprint doi: <https://doi.org/10.1101/2020.08.10.243998>*.
- Schumann, A., de la Cruz, F., Kohler, S., Brotte, L., Bar, K.J., 2021. The influence of heart rate variability biofeedback on cardiac regulation and functional brain connectivity. *Front. Neurosci.* 15, 691988.
- Seeley, W.W., 2019. The salience network: a neural system for receiving and responding to homeostatic demands. *J. Neurosci.* 39, 9878–9882.
- Seghier, M.L., Friston, K.J., 2013. Network discovery with large DCMs. *Neuroimage* 68, 181–191.
- Shaffer, F., Ginsberg, J.P., 2017. An overview of heart rate variability metrics and norms. *Front. Public Health* 5, 258.
- Shaffer, F., McCraty, R., Zerr, C.L., 2014. A healthy heart is not a metronome: an integrative review of the heart's anatomy and heart rate variability. *Front. Psychol.* 5, 1040.
- Sklerov, M., Dayan, E., Browner, N., 2019. Functional neuroimaging of the central autonomic network: recent developments and clinical implications. *Clin. Auton. Res.* 29, 555–566.
- Smith, D.M., Torregrossa, M.M., 2021. Valence encoding in the amygdala influences motivated behavior. *Behav. Brain Res.* 411, 113370.
- Smith, S.M., Fox, P.T., Miller, K.L., Glahn, D.C., Fox, P.M., Mackay, C.E., Filippini, N., Watkins, K.E., Toro, R., Laird, A.R., Beckmann, C.F., 2009. Correspondence of the brain's functional architecture during activation and rest. *Proc. Natl. Acad. Sci. U.S.A.* 106, 13040–13045.
- Smith, S.M., Miller, K.L., Salimi-Khorshidi, G., Webster, M., Beckmann, C.F., Nichols, T.E., Ramsey, J.D., Woolrich, M.W., 2011. Network modelling methods for fMRI. *Neuroimage* 54, 875–891.
- Smitha, K.A., Akhil Raja, K., Arun, K.M., Rajesh, P.G., Thomas, B., Kapilamoorthy, T.R., Kesavadas, C., 2017. Resting state fMRI: a review on methods in resting state connectivity analysis and resting state networks. *Neuroradiol. J.* 30, 305–317.
- Sripada, R.K., King, A.P., Garfinkel, S.N., Wang, X., Sripada, C.S., Welsh, R.C., Liberzon, I., 2012. Altered resting-state amygdala functional connectivity in men with posttraumatic stress disorder. *J. Psychiatry Neurosci.* 37, 241–249.
- Stein, P.K., Bosner, M.S., Kleiger, R.E., Conger, B.M., 1994. Heart rate variability: a measure of cardiac autonomic tone. *Am. Heart. J.* 127, 1376–1381.
- Stephan, K.E., Penny, W.D., Daunizeau, J., Moran, R.J., Friston, K.J., 2009. Bayesian model selection for group studies. *Neuroimage* 46, 1004–1017. PMID: 19306932.
- Taren, A.A., Gianaros, P.J., Greco, C.M., Lindsay, E.K., Fairgrieve, A., Brown, K.W., Rosen, R.K., Ferris, J.L., Julson, E., Marsland, A.L., Burley, J.K., Ramsburg, J., Creswell, J.D., 2015. Mindfulness meditation training alters stress-related amygdala resting state functional connectivity: a randomized controlled trial. *Soc. Cogn. Affect. Neurosci.* 10, 1758–1768.
- Tarvainen, M.P., Niskanen, J.P., Lipponen, J.A., Ranta-Aho, P.O., Karjalainen, P.A., 2014. Kubios HRV—heart rate variability analysis software. *Comput. Methods Programs Biomed.* 113, 210–220.
- Thayer, J.F., Ahs, F., Fredrikson, M., Sollers 3rd, J.J., Wager, T.D., 2012. A meta-analysis of heart rate variability and neuroimaging studies: implications for heart rate variability as a marker of stress and health. *Neurosci. Biobehav. Rev.* 36, 747–756.
- Thayer, J.F., Lane, R.D., 2009. Claude Bernard and the heart-brain connection: further elaboration of a model of neurovisceral integration. *Neurosci. Biobehav. Rev.* 33, 81–88.
- Vaisvilaite, L., Hushagen, V., Gronli, J., Specht, K., 2022. Time-of-day effects in resting-state functional magnetic resonance imaging: changes in effective connectivity and blood oxygenation level dependent signal. *Brain Connect.* 12, 515–523.
- Valenza, G., Passamonti, L., Duggento, A., Toschi, N., Barbieri, R., 2020. Uncovering complex central autonomic networks at rest: a functional magnetic resonance imaging study on complex cardiovascular oscillations. *J. R. Soc. Interface* 17, 20190878.
- Van Overwalle, F., Van de Steen, F., Marien, P., 2019. Dynamic causal modeling of the effective connectivity between the cerebrum and cerebellum in social mentalizing across five studies. *Cogn. Affect. Behav. Neurosci.* 19, 211–223.
- Vanneste, S., De Ridder, D., 2013. Brain areas controlling heart rate variability in tinnitus and tinnitus-related distress. *PLoS. One* 8, e59728.
- Wadden, K.P., Snow, N.J., Sande, P., Slawson, S., Waller, T., Boyd, L.A., 2018. Yoga practitioners uniquely activate the superior parietal lobe and supramarginal gyrus during emotion regulation. *Front. Integr. Neurosci.* 12, 60.
- Wager, T.D., Waugh, C.E., Lindquist, M., Noll, D.C., Fredrickson, B.L., Taylor, S.F., 2009. Brain mediators of cardiovascular responses to social threat: part I: reciprocal dorsal and ventral sub-regions of the medial prefrontal cortex and heart-rate reactivity. *Neuroimage* 47, 821–835.
- Wehrwein, E.A., Orer, H.S., Barman, S.M., 2016. Overview of the anatomy, physiology, and pharmacology of the autonomic nervous system. *Compr. Physiol.* 6, 1239–1278.
- Wei, L., Chen, H., Wu, G.R., 2018. Structural covariance of the prefrontal-amygdala pathways associated with heart rate variability. *Front. Hum. Neurosci.* 12, 2.
- White, D.W., Raven, P.B., 2014. Autonomic neural control of heart rate during dynamic exercise: revisited. *J. Physiol.* 592, 2491–2500.
- Whitfield-Gabrieli, S., Nieto-Castanon, A., 2012. Conn: a functional connectivity toolbox for correlated and anticorrelated brain networks. *Brain Connect.* 2, 125–141.
- Woisard, K., Steinberg, J.L., Ma, L., Zuniga, E., Ramey, T., Lennon, M., Keyser-Marcus, L., Moeller, F.G., 2021. Preliminary findings of weaker executive control network resting state fMRI functional connectivity in opioid use disorder compared to healthy controls. *J. Addict. Res. Ther.* 12.
- Woolrich, M.W., Behrens, T.E., Beckmann, C.F., Jenkinson, M., Smith, S.M., 2004. Multilevel linear modelling for fMRI group analysis using Bayesian inference. *Neuroimage* 21, 1732–1747.
- Xia, M., Wang, J., He, Y., 2013. BrainNet Viewer: a network visualization tool for human brain connectomics. *PLoS. One* 8, e68910.
- Young, H.A., Benton, D., 2018. Heart-rate variability: a biomarker to study the influence of nutrition on physiological and psychological health? *Behav. Pharmacol.* 29, 140–151.
- Young, H.A., Cousins, A., Johnston, S., Fletcher, J.M., Benton, D., 2019. Autonomic adaptations mediate the effect of hydration on brain functioning and mood: evidence from two randomized controlled trials. *Sci. Rep.* 9, 16412.
- Young, K.D., Siegle, G.J., Misaki, M., Zotev, V., Phillips, R., Drevets, W.C., Bodurka, J., 2018. Altered task-based and resting-state amygdala functional connectivity following real-time fMRI amygdala neurofeedback training in major depressive disorder. *Neuroimage Clin.* 17, 691–703.
- Zeidman, P., Jafarian, A., Corbin, N., Seghier, M.L., Razi, A., Price, C.J., Friston, K.J., 2019. A guide to group effective connectivity analysis, part 1: first level analysis with DCM for fMRI. *Neuroimage* 200, 174–190.